Journal of Microscopy, Vol. 196, Pt 2, November 1999, pp. 185–193.
Received 9 June 1998; accepted 15 April 1999

Carbon-fibre reinforced magnesium alloys: nanostructure and chemistry of interlayers and their effect on mechanical properties

A. FELDHOFF, E. PIPPEL & J. WOLTERSDORF
Max-Planck-Institut für Mikrostrukturphysik, Weinberg 2, D-06120 Halle, Germany

Key words. Al_4C_3, Al_2MgC_2, C/Mg–Al, carbide formation, carbon fibre, electron energy loss spectroscopy, ELNES, interface reactivity, interface structure, MMC, transmission electron microscopy.

Summary

The micromechanical fracture behaviour of C/Mg–Al composites of varying interface reactivity was investigated by scanning electron microscope bending tests. Structure and chemistry of fibre/matrix interlayers were studied down to the atomic scale by imaging and spectroscopical transmission electron microscope techniques (high-resolution electron microscopy, energy dispersive X-ray spectroscopy, parallel-recording electron energy loss spectroscopy and energy-filtered transmission electron microscopy). The chemical reactions at the fibre/matrix interfaces of the C/Mg–Al composites were found to form plate-shaped carbidic precipitates, mainly Al_2MgC_2, which strongly influence the composite's mechanical properties by changing the fibre/matrix bonding strength.

1. Introduction

Metal matrix composites (MMCs) of the system carbon fibre/magnesium alloy promise outstanding mechanical properties owing to the low density of their components (approx. $1{\cdot}8\,\mathrm{g\,cm^{-3}}$) and the high strength of carbon fibres (3–4 GPa). As the effectiveness of the fibre-reinforcement in an MMC depends sensitively on the properties of the interlayers between the components, optimum parameters of the composite material can only be attained by tailoring the fibre/matrix interface, including a reduction in fibre degradation.

In the chemical literature (Irmann, 1948; Schneider & Cordes, 1955; Hájek *et al.*, 1983a, 1983b), the system C/Mg is treated as a chemically non-reactive one. This is because the two binary magnesium carbides MgC_2 and Mg_2C_3 are endothermic compounds which start to decompose at about 500 °C and 650 °C, respectively. Therefore, the formation of MgC_2 or Mg_2C_3 at temperatures of the MMC processing (700–800 °C) seems to be very unlikely, implying a good compatibility of the MMC components. Otherwise, the non-reactive character of the system C/Mg leads to a very weak bonding between fibre and matrix. In principle (Delannay *et al.*, 1987), the desired adjustment of the interfacial bonding can be accomplished by creating reactive conditions via changing the chemistry of the fibre surface or of the matrix. A favourable alloying element to increase the interface reactivity is aluminium, which forms the stable binary carbide Al_4C_3 (Qui & Metselaar, 1994) or may lead to the formation of the ternary carbides Al_2MgC_2 (Viala *et al.*, 1991) or $Al_4Mg_2C_3$ (Flower & Morris, 1987). Moreover, it is the technologically most important alloying element for magnesium.

In general, insight into the chemical interface kinetics during the composite manufacturing process and into the correlation of interface structures with mechanical properties helps to optimize the materials. Therefore, structure and chemistry of fibre/matrix interlayers in C/Mg–Al composites of varying interface reactivity have been studied down to the atomic scale by different transmission electron microscope techniques (imaging and spectroscopical methods). The fracture behaviour of the composites was studied by scanning electron microscopical three-point bending tests.

2. Experimental

Unidirectionally carbon-fibre reinforced magnesium/aluminium alloys with a fibre content of approx. 63 vol.% were produced at the University of Erlangen via a gas-pressure melt-infiltration process (Öttinger & Singer, 1993) for a 5-min fibre/melt contact at 720 °C. Two types of commercially

Correspondence to: A. Feldhoff. Tel: +49 345 5582 926; fax: +49 345 5511 223; e-mail: feldhoff@mpi-halle.mpg.de

available sized polyacrylonitrile-base carbon fibre (Toray) with different surface microstructures and therefore different reactivities were used as reinforcements: M40J as a high-modulus type, with the outermost graphite basal planes in preferentially parallel orientation to the relatively smooth surface (low reactivity), and T300J as a high-tensile-strength type, with many free-ending graphite basal planes at the rougher surface (high reactivity). Magnesium alloys with different amounts of the carbide-forming element Al were used as matrices: AM20 (2 wt.% Al and 0·4 wt.% Mn) and AZ91 (9 wt.% Al and 0·7 wt.% Zn). In order of increasing fibre/matrix reactivity, the three composites M40J/AM20, T300J/AM20 and T300J/AZ91 were studied.

For three-point bending tests, a special microbending-stage (Raith, Dortmund) was incorporated in an environmental scanning electron microscope (ESEM-3, Electro Scan, Wilmington) to enable the *in-situ* observation of the respective damage evolution (Feldhoff *et al.*, 1995). For localizing the stress intensities, 100 μm deep notches were sawn in the middle of the rectangular specimens ($23 \times 5 \times 1{\cdot}5\,\text{mm}^3$) using a 50-$\mu$m tungsten wire saw.

For the bending geometry used (specimen width $a = 5$ mm, specimen thickness $b = 1{\cdot}5$ mm, span length $s = 17$ mm), the bending strength σ_b can be estimated from the load maximum $F_{\max}$ using the formula

$$\sigma_b = \frac{3}{2}\frac{F_{\max} \cdot s}{a \cdot b^2},$$

leading to the relation $\sigma_b\,[\text{MPa}] \approx 2{\cdot}27\,F_{\max}\,[\text{N}]$. Of course, the bending strength of non-notched samples would be higher than the values estimated here. The fracture surfaces of broken specimens were examined in a scanning electron microscope of the type Jeol JSM-6300F.

For transmission electron microscope (TEM) investigations, MMC specimens were prepared, using a water-free lubricant, by cutting thin (500 μm) slices 3 mm in diameter perpendicular to the fibre axis, planar grinding and double-mould dimpling to a thickness of about 20 μm, followed by ion milling (Ar, 5 kV) down to electron transparency (Feldhoff, 1998). For TEM investigation of Al_4C_3 standard samples, a powder (Aldrich, purity 99·999%, − 325 mesh) was crushed in a mortar and dispersed onto a supporting grid using methanol.

For high-resolution electron microscopy (HREM), selected area diffraction (SAD), energy dispersive X-ray spectroscopy, electron energy loss spectroscopy (EELS), and energy-filtered transmission electron microscopy (EFTEM), a combined (scanning) transmission electron microscope of the type Philips CM 20 FEG operated at 200 kV was used; this was equipped with a light element X-ray detector (Tracor Voyager II), and a parallel-recording energy loss spectrometer (Gatan PEELS model 666) or an imaging energy filter (Gatan Image Filter GIF 200), respectively. According to the characteristics of the thermally assisted field emission gun the energy resolution of EELS (full-width at half maximum of the zero-loss peak) amounted to about 0·8 to 1 eV. In general, EEL spectra were acquired with a dispersion of 0·5 eV per channel before they were deconvoluted with the zero-loss peak to improve the resolution. To minimize the contamination effects, which are generally strong for small electron probes of some nanometres, a cooling specimen holder (Gatan model 668) was used during the analytical procedures. Information on the chemical bond state of the elements present was gained by analysing energy loss near-edge structures (ELNES), which can be attributed to transitions of core-shell electrons into unoccupied states above the Fermi level (Brydson *et al.*, 1991; Rez, 1992). Characteristic ELNES details used are the edge onset as well as the shape, the energy position and the intensity of the individual features in the fine-structure.

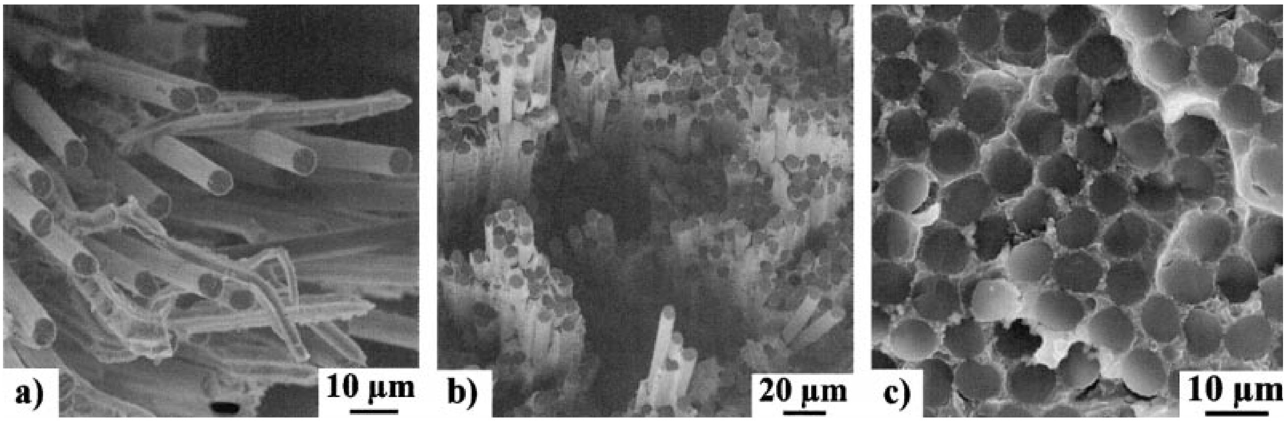

Fig. 1. SEM images of the fracture surfaces of the composites: (a) M40J/AM20; (b) T300J/AM20; (c) T300J/AZ91.

Table 1. Results of the three-point bending tests, obtained from notched samples and single tests.

Material	Fibre/matrix reactivity	Maximum load (N)	Bending strength (MPa)	Fracture mode
M40J/AM20	Low	240	544	Single fibre pullout
T300J/AM20	Medium	410	929	Bundle fracture
T300J/AZ91	High	70	158	Brittle fracture

3. Results

3.1. Micromechanics of the composites

Figure 1 shows the tensile stress subjected parts of the fracture surfaces of the MMCs exhibiting three different fracture modes depending on the interface reactivity. Composite M40J/AM20 (Fig. 1a) failed owing to single fibre pullout. A weak interface bonding is indicated by single fibres which are debonded from the matrix and stick out from the fracture surface. Composite T300J/AM20 (Fig. 1b) failed due to bundle fracture. Its fracture surface is characterized by individual bundles of up to 80 fibres, within which the fibres are bonded together by the matrix metal. The fracture surface of composite T300J/AZ91 (Fig. 1c) is relatively flat, indicating a brittle fracture as is known for monolithic ceramics.

The three failure patterns correlate with different load maxima $F_{\max}$, and therefore different bending strengths σ_b, which are listed in Table 1. The load deflection diagrams were presented by Feldhoff *et al.* (1997) and Hähnel *et al.* (1997). Obviously, neither a very low (M40J/AM20) nor a very high interface reactivity (T300J/AZ91) is favourable for the composite material. In both cases the composite strength is low. A high strength ($\sigma_b = 929$ MPa) is observed only in composite T300J/AM20, with a medium interface reactivity.

3.2. Microstructure of the composites

In composite M40J/AM20, of low interface reactivity, no carbides have formed. Rather, an oxygen-containing interlayer was observed: the bright-field image of the fibre/matrix interface in Fig. 2(a) shows that the fibre exhibits many pores of 5–10 nm in diameter below its surface. Figure 2(b) shows the corresponding superimposed elemental maps of carbon (red), oxygen (green) and magnesium (blue) obtained by EFTEM using the corresponding K ionization edges, thus revealing an oxygen-containing interlayer. HREM images proved that the interlayer consists of crystallites of 5–10 nm in diameter showing lattice fringes of 0·21 nm, which can be attributed to MgO (Feldhoff *et al.*, 1997; Feldhoff, 1998). Locally, the thickness of the nanocrystalline MgO interlayer varied from 10 to 50 nm. The pores in the M40J fibre were found in regions up to 200 nm below the fibre surface, in the as-received fibre as well as in the composite (Feldhoff, 1998). They may result from oxidative surface treatments during the fibre production as described in the papers by Weiss (1989), Krekel *et al.* (1994), and Mahy *et al.* (1994). Usually, fibres of the high-modulus type are subjected to these surface treatments for longer periods than those of the high-tensile-strength type. Accordingly, the T300J fibre did not exhibit such large pores (Feldhoff, 1998). Probably, the pores in the surface near regions of the M40J fibre are a source for oxygen, thus

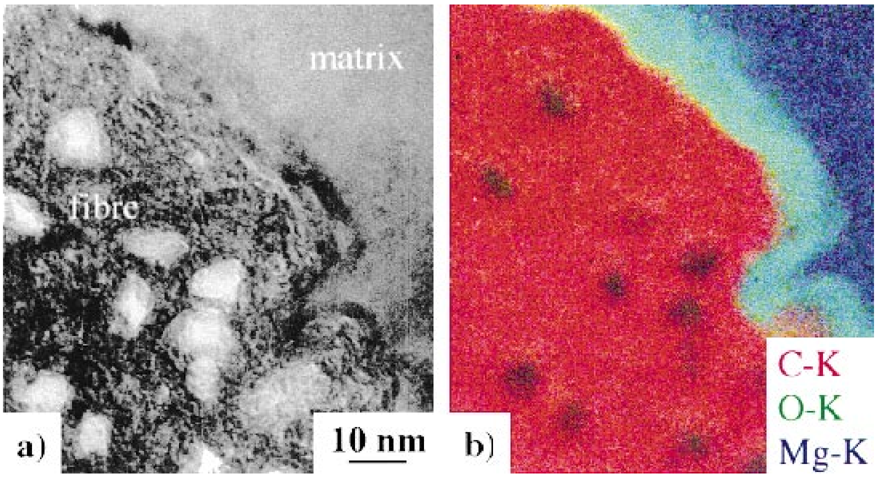

Fig. 2. Fibre/matrix interface in composite M40J/AM20: (a) TEM bright-field image; (b) EFTEM using the K ionization edges of carbon, oxygen and magnesium.

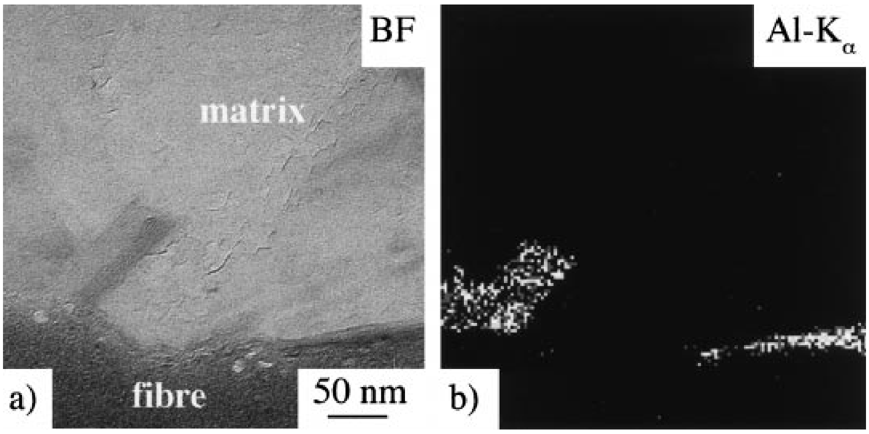

Fig. 3. Fibre/matrix interface in composite T300J/AM20: (a) TEM bright-field image; (b) intensity map of Al–K$_\alpha$ X-rays (represented by white pixels).

explaining why the phenomenon of an MgO interlayer has not been observed in the composites containing the T300J fibre.

The bright-field image of Fig. 3(a) shows some precipitates at the fibre/matrix interface of composite T300J/AM20. The intensity map of Al-K$_\alpha$ X-rays in Fig. 3(b) reveals that aluminium is concentrated in them. Usually, the precipitates in T300J/AM20 are shorter than 100 nm.

In composite T300J/AZ91, with the high aluminium content of 9 wt.% of the matrix, more and even larger precipitates have formed (Fig. 4a). The elemental map of aluminium in Fig. 4(b) clearly shows that they cover the fibre surface completely, with some reaching up to 1 μm into the matrix.

In composite T300J/AZ91, some precipitates have been identified as the binary carbide Al_4C_3. In the HREM images, they showed a (0003) lattice fringe distance of 0·83 nm. However, in most cases, the precipitates showed a lattice fringe distance of 0·62 nm. In composite T300J/AM20, only this second kind of precipitate occurred (Feldhoff, 1998). Often, these precipitates did not grow regularly, as the left part of Fig. 5 shows. Instead, they exhibited many planar defects parallel to their (0001) basal plane (right part of Fig. 5).

3.3. Nanoanalysis of carbidic precipitates

As the micromechanical behaviour of the composites (section 3.1) correlates with the amount and size of precipitates at the fibre/matrix interface (section 3.2), the

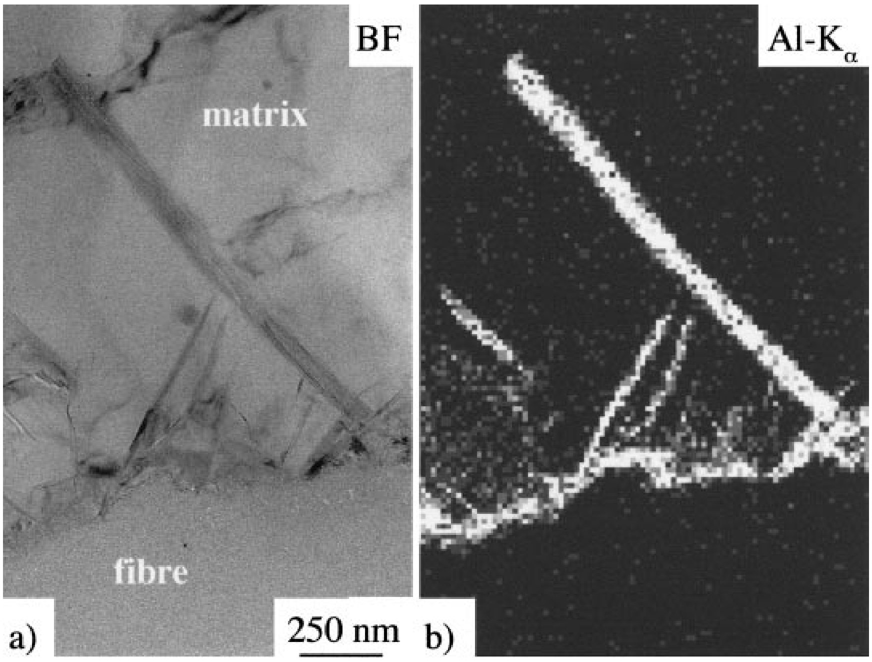

Fig. 4. Fibre/matrix interface in composite T300J/AZ91: (a) TEM bright-field image; (b) intensity map of Al–K$_\alpha$ X-rays (represented by white pixels).

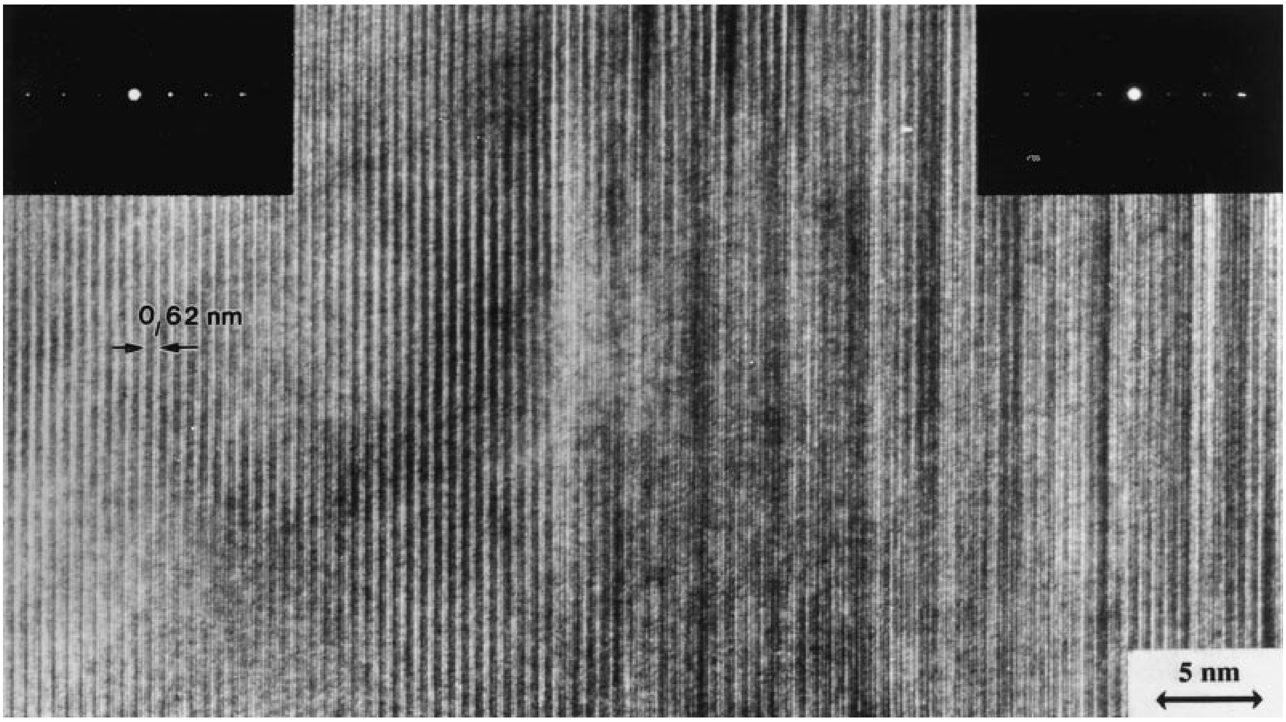

Fig. 5. HREM image of a precipitate in T300J/AZ91, with the *c*-axes in perpendicular orientation to the electron beam, and corresponding SAD pattern.

optimization of C/Mg–Al materials requires the analysis of their nature. In the following, results of EELS investigations on the defect-free part of a precipitate (left part of Fig. 5) are described. ELNES is used to reveal the chemical coordination of the individual elements (Schneider *et al.*, 1996, 1997). Based on this, these fine structures of the ionization edges are compared to those of standard substances in the sequence Mg–L_{23} and Mg–K, Al–L_{23} and Al–K and C–K.

The EEL spectrum of the precipitate reveals an Mg–L_{23} ionization edge (Fig. 6a) and an Mg–K one (Fig. 6b), with their ELNES differing from those of standard metallic Mg and MgO. As to the precipitate phase in Fig. 6(a), there is an Al–L_{23} edge, with an onset energy at about 73·5 eV, superimposed on the Mg–L_{23} ELNES. It originates from aluminium atoms in the vicinity of magnesium atoms. In Fig. 7(a), the Al–L_{23} ELNES of the precipitate is compared to different aluminium compounds. From bottom to top, the spectra are arranged in increasing order of onset energy, i.e. with the oxidation state of aluminium increasing. The Al–L_{23} ELNES of the Al_4C_3 standard and of the precipitate phase differ distinctly from that of metallic aluminium and aluminium oxide (Fig. 7a). They mainly correspond to one another, however. In both cases, the onset energy is at about 73·5 eV. After a steep rise of the signal there follows a relatively broad peak at about 77·5 eV. In both spectra, broader peaks occur with higher energy losses: for the Al_4C_3 standard, at about 98·5 eV and for the precipitate phase, at about 100 eV. Near the Al–K ionization edge (Fig. 7b), the spectra of Al_4C_3 and of the precipitate do not show any remarkable differences in the bonding-specific fine-structure features. However, both again differ clearly from those of metallic aluminium and aluminium oxide. Their onset energies are at 1565 eV, accompanied by a peak at about 1573 eV and by one of lower intensity at about 1584 eV. The latter peak does not occur in the spectra of metallic Al and of Al_2O_3.

As common fine-structure features, the C–K ionization edges of the Al_4C_3 standard and of the precipitate (Fig. 8) exhibit the same onset energy at 283 eV as well as two pronounced peaks, at 291 eV and near 300 eV, respectively. Differences occur in the position of the maximum of the second peak, which for Al_4C_3 is at 305 eV, for the precipitate at 302 eV, and at about 287 eV near the first peak, where the slope of the precipitate decreases.

From the distinct similarities of the ELNES between the Al_4C_3 standard and the precipitate phase at the Al–L_{23}, Al–K and C–K ionization edges it can be concluded that the chemical environments of the elements in both compounds are similar in each case. This points to a close relationship in the crystal chemistry of both the Al–Mg–C precipitate and the binary carbide Al_4C_3.

The lattice fringe contrast of 0·62 nm of the precipitates (Fig. 5) can be attributed to the (0002) lattice spacing of a polymorph of Al_2MgC_2 of hexagonal crystal symmetry, which

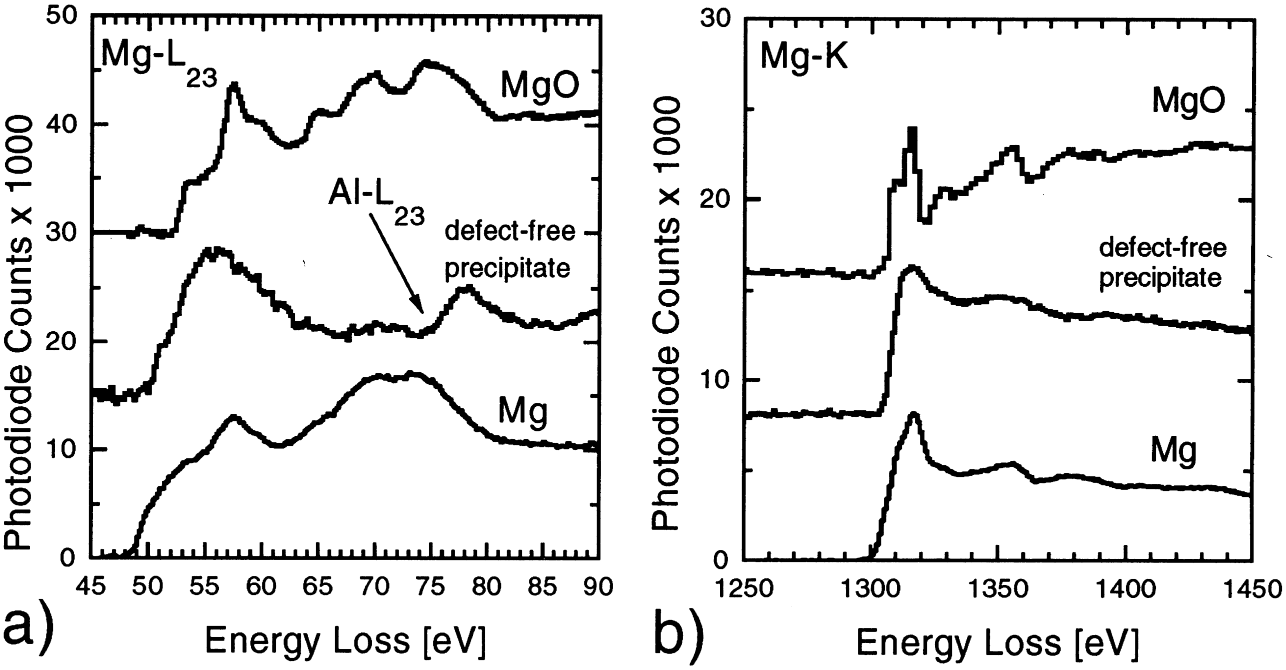

Fig. 6. EEL spectra of the defect-free precipitate compared to standard substances: (a) Mg–L$_{23}$ ELNES; (b) Mg–K ELNES.

was synthesized and investigated via X-ray diffractometry by Viala *et al.* (1991). A structural model for this ternary carbide was proposed by Feldhoff (1998). In Fig. 9, the atomic arrangement of Al_2MgC_2 projected on the $(11\bar{2}0)$ plane is compared to the well-known arrangement (Jeffrey & Wu, 1963; Gesing & Jeitschko, 1995) of the binary carbide Al_4C_3. The crystal structures are related to each other by a substitution of hexagonal close-packed (h) aluminium double layers (Al_4C_3), which have carbon atoms in the trigonal-bipyramidal interstices, by single layers of magnesium, again in an hexagonal close-packed stacking (Al_2MgC_2). Common to both structures are double layers of aluminium in a cubic close-packed stacking (c), with carbon atoms in octahedral interstices between them. This close

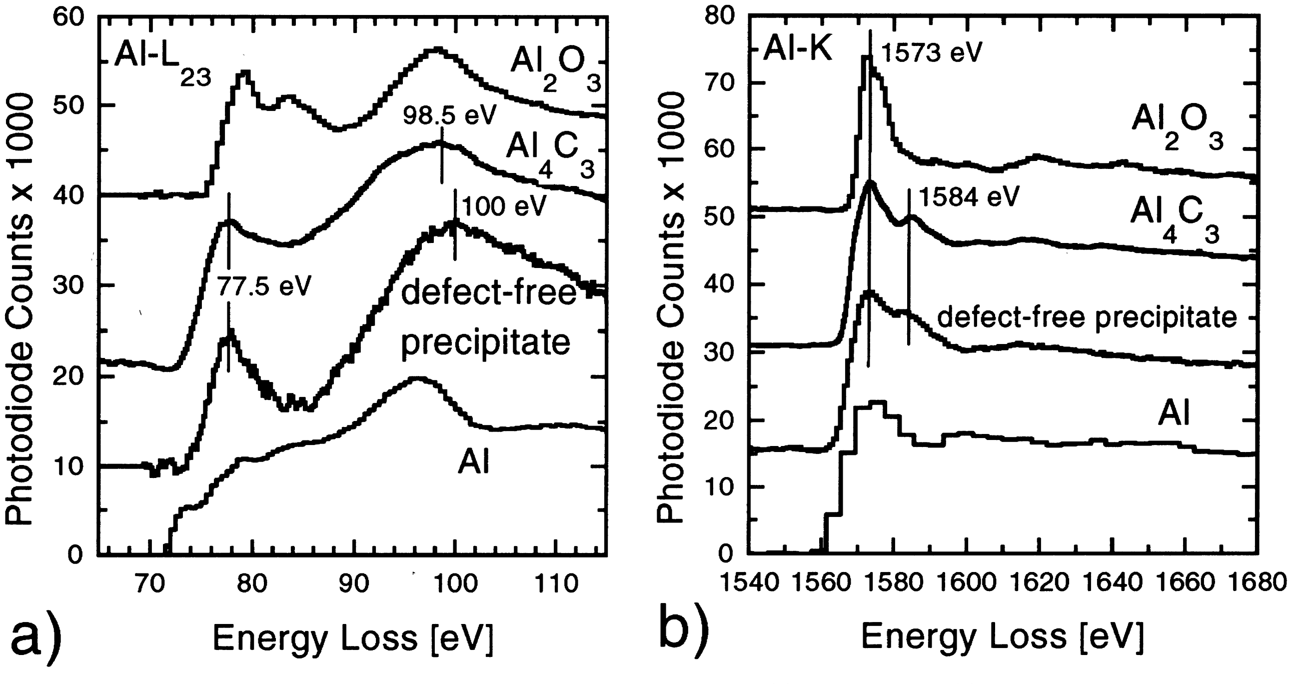

Fig. 7. EEL spectra of the defect-free precipitate compared to standard substances: (a) Al–L$_{23}$ ELNES; (b) Al–K ELNES.

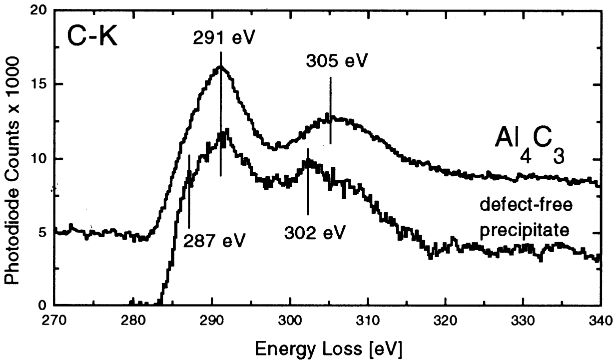

Fig. 8. C–K ELNES of the defect-free precipitate compared to Al_4C_3.

relationship in the crystal chemistry of ternary Al_2MgC_2 and binary Al_4C_3 may explain the observed similarities of the ELNES features of aluminium (Fig. 7) and carbon (Fig. 8).

3.4. Morphology and growth of Al_2MgC_2 precipitates

The Al_2MgC_2 precipitates at the fibre/matrix interfaces of the investigated C/Mg–Al composites are plate-shaped, i.e. they are laterally extended always in perpendicular orientation to their [0001] direction. In Fig. 10, the lattice fringe image of a plate-shaped ternary carbide shows that the carbide basal faces (parallel to the (0001) planes) are atomically flat, whereas the side faces are atomically rough, with many growth ledges. This morphology of Al_2MgC_2 precipitates in C/Mg–Al composites resembles that of Al_4C_3 in C/Al systems, which was investigated by Gu *et al.* (1994, 1996) and Yang *et al.* (1996). Therefore, by analogy to Al_4C_3 in a matrix of pure Al, growth mechanisms are assumed for Al_2MgC_2 in a magnesium-rich Mg–Al matrix: in directions normal to the rough interfaces (perpendicular to the *c*-axis of the carbide) the crystal growth is diffusion controlled, and in direction normal to the flat interface (parallel to the *c*-axis) the growth proceeds by an interface-controlled ledge mechanism, which is much slower. The difference in the velocities of the two growth modes always causes the formation of plate-shaped carbide precipitates.

4. Conclusions

The chemical reactions at the fibre/matrix interfaces of C/Mg–Al composites proved to form plate-shaped carbidic precipitates, mainly Al_2MgC_2 (but also some Al_4C_3). Amount and size of the carbides depend on the interface reactivity and strongly influence the mechanical composite properties by changing the fibre/matrix bonding strength. Large carbidic plates may also affect the fibre strength by deleterious notching effects. An optimized material can be achieved by a moderate interface reactivity and is characterized by a bundle fracture behaviour.

Acknowledgements

The authors would like to thank Professor R. F. Singer and Dr O. Öttinger (University of Erlangen-Nürnberg) for

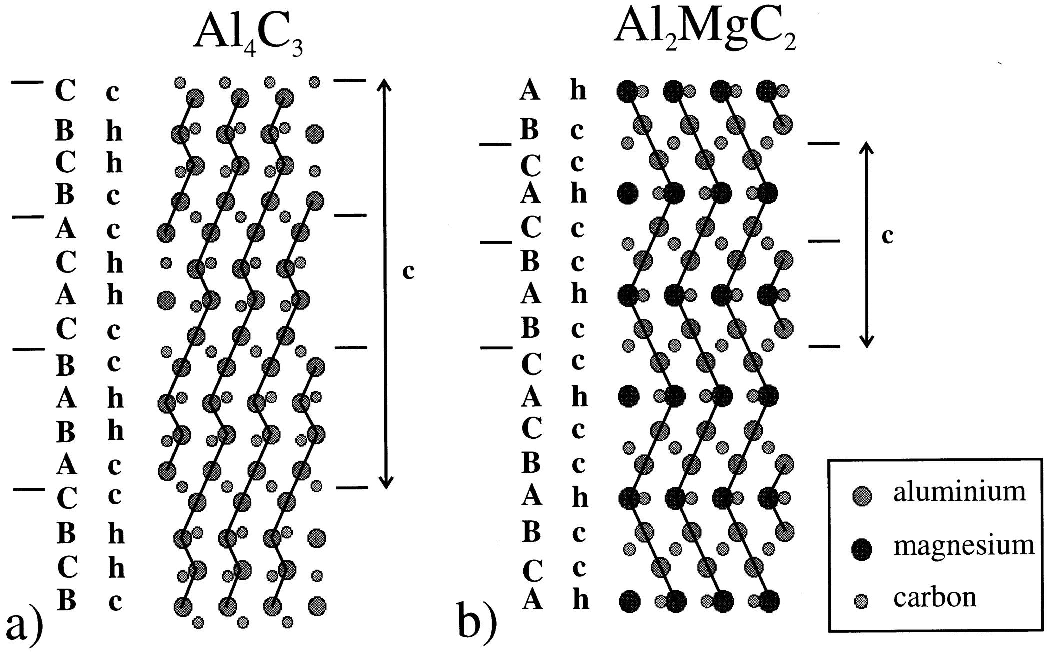

Fig. 9. Structures of the carbides represented by cuts along the $(11\bar{2}0)$ planes: (a) Al_4C_3; (b) Al_2MgC_2 (structural proposal).

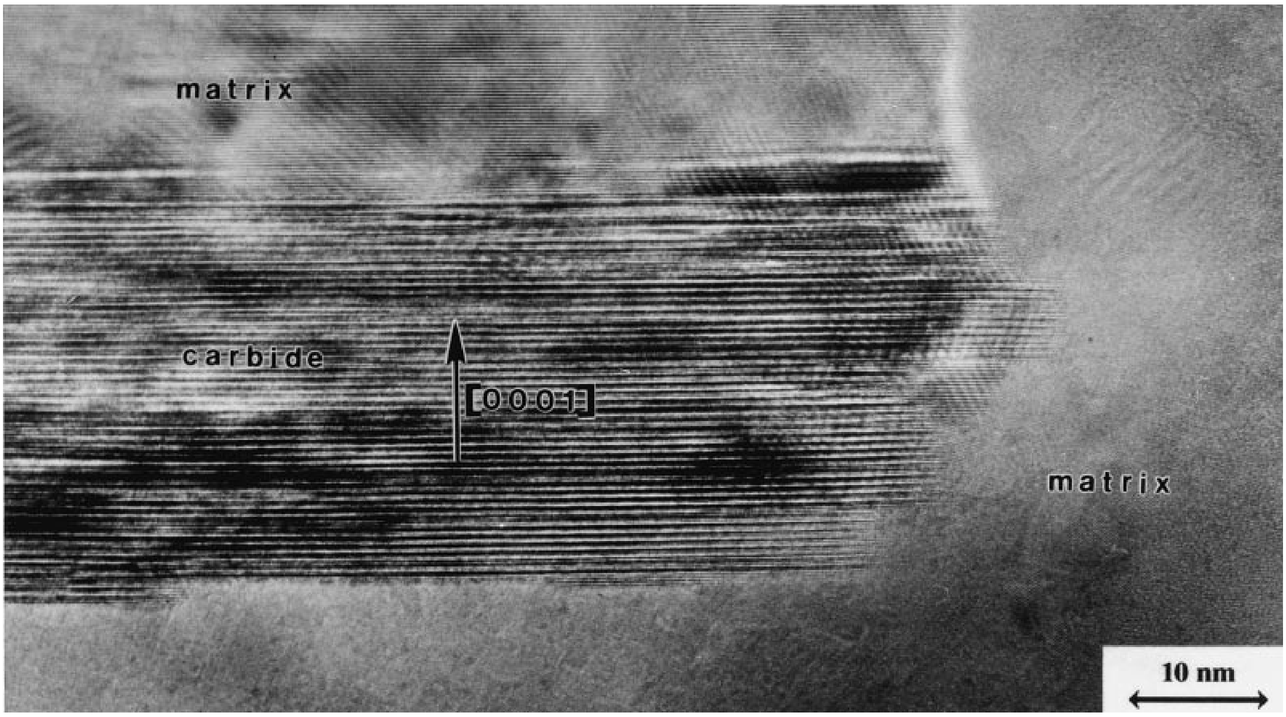

Fig. 10. Carbidic precipitate in the matrix of T300J/AZ91, with its *c*-axis in perpendicular orientation to the electron beam.

providing the MMC samples, Dr M. Füting (Fraunhofer Institute for Mechanics of Materials, Branchlab Halle) for placing the provision of the ESEM-3/bending stage and their colleague Dr R. Schneider for his support in recording EEL spectra.

References

Brydson, R., Sauer, H., Engel, W. & Zeitler, E. (1991) EELS as a fingerprint of the chemical co-ordination of light elements. *Microsc. Microanal. Microstruct.* **2,** 159–169.

Delannay, F., Froyen, L. & Deruytters, A. (1987) Review: the wetting of solids by molten metals and its relation to the preparation of metal–matrix composites. *J. Mater. Sci.* **22,** 1850–1861.

Feldhoff, A. (1998) *Beiträge zur Grenzschichtoptimierung im Metall-Matrix-Verbund Carbonfaser/Magnesium*. PhD Thesis, Martin Luther University of Halle-Wittenberg 1997, Shaker Verlag, Aachen-Maastricht.

Feldhoff, A., Pippel, E. & Woltersdorf, J. (1995) *The role of interface reactions in the fracture behaviour of fibre-reinforced metals – EM in-situ bending tests of carbon/Mg-Al alloys*. Video Tape, MPI für Mikrostrukturphysik, Halle.

Feldhoff, A., Pippel, E. & Woltersdorf, J. (1997) Interface reactions and fracture behaviour of fibre-reinforced Mg/Al alloys. *J. Microsc.* **185,** 122–131.

Flower, H.M. & Morris, A.J. (1987) Magnox oxidation in carbon dioxide. *Conference: Magnesium Technology, London, UK, 3–4 November 1986* (ed. by C. Baker), pp. 128–132, The Institute of Metals, London.

Gesing, T.M. & Jeitschko, W. (1995) The crystal structure and chemical properties of $U_2Al_3C_4$ and structure refinement of Al_4C_3. *Z. Naturforsch. B*, **50,** 196–200.

Gu, M., Yang, H., Jiang, W. & Zhang, G. (1994) Interfacial structure characterization of C/Al composites. *High Performance Composites: Commonalty of Phenomena* (ed. by K. K. Chawla, P. K. Liaw and S. G. Fishman), pp. 121–127. The Minerals, Metals & Materials Society, Warrendale, PA.

Gu, M., Yang, H., Jiang, W. & Zhang, G. (1996) Study on the interfacial reaction product in Gr/Al composites. *Adv. Composite Mater.* **5** (2), 119–128.

Hähnel, A., Pippel, E., Feldhoff, A., Schneider, R. & Woltersdorf, J. (1997) Reaction layers in MMCs and CMCs: structure, composition and mechanical properties. *Mater. Sci. Eng.* **A237,** 173–179.

Hájek, B., Karen, P. & Brozek, V. (1983a) Thermal decomposition of magnesium sesquicarbide. *Coll. Czech. Chem. Commun.* **48** (7), 1963–1968.

Hájek, B., Karen, P. & Brozek, V. (1983b) Synthesis and thermal decomposition of magnesium dicarbide. *Coll. Czech. Chem. Commun.* **48** (7), 1969–1976.

Irmann, F. (1948) Zur Kenntnis der Magnesiumcarbide. *Helv. Chim. Acta*, **31,** 1584–1602.

Jeffrey, G.A. & Wu, V.Y. (1963) The structures of the aluminium carbonitrides. *Acta Crystallogr.* **16,** 559–566.

Krekel, G., Hüttinger, K.J., Hoffmann, W.P. & Silver, D.S. (1994) The relevance of the surface structure and surface chemistry of carbon fibres in their adhesion to high-temperature thermoplastics. *J. Mater. Sci.* **29,** 2968–2980.

Mahy, J., Jenneskens, L.W., Grabandt, O., Venema, A. & van

Houwelingen, G.D.B. (1994) The relation between carbon-fibre surface treatment and the fibre surface microstructure. *Surf. Interface Anal.* **21,** 1–13.

Öttinger, O. & Singer, R.F. (1993) An advanced melt infiltration process for the net shape production of metal matrix composites. *Z. Metallkunde*, **84,** 827–831.

Qui, C. & Metselaar, R. (1994) Solubility of carbon in liquid aluminium and stability of Al_4C_3. *J. Alloys Comp.* **216,** 55–60.

Rez, P. (1992) Energy loss fine structure. *Transmission Electron Energy Loss Spectrometry in Materials Science* (ed. by M. M. Disko, C. C. Ahn and B. Fultz), pp. 107–129, The Minerals, Metals & Materials Society, Warrendale, PA.

Schneider, A. & Cordes, J.F. (1955) Zur Darstellung und thermischen Stabilität der Magnesiumcarbide MgC_2 und Mg_2C_3. *Z. anorg. allg. Chem.* **279,** 94–103.

Schneider, R., Woltersdorf, J. & Lichtenberger, O. (1996) ELNES across interlayers in SiC (Nicalon) fibre-reinforced Duran glass. *J. Phys. D: Appl. Phys.* **29,** 1709–1715.

Schneider, R., Woltersdorf, J. & Röder, A. (1997) EELS nanoanalysis for investigating both chemical composition and bonding of interlayers in composites. *Microchim. Acta*, **125,** 361–365.

Viala, J.C., Bosselet, F., Claveyrolas, G., Mentzen, B.F. & Bouix, J. (1991) Characterization of two new crystalline phases in the Al-C-Mg system. *Eur. J. Solid State Inorg. Chem.* **28** (5), 1063–1070.

Weiss, R. (1989) Modellvorstellungen über die Haftung bei C-faserverstärkten Polymeren mit duromerer und thermoplastischer Matrix. *Haftung bei Verbundwerkstoffen und Werkstoffverbunden* (ed. by W. Brockmann), pp. 195–220, DGM Informationsgesellschaft, Oberursel.

Yang, H., Gu, M., Jiang, W. & Zhang, G. (1996) Interface microstructure and reaction in Gr/Al metal matrix composites. *J. Mater. Sci.* **31,** 1903–1907.